Journal of Power Sources 195 (2010) 2008–2013

Contents lists available at ScienceDirect

Journal of Power Sources

journal homepage: www.elsevier.com/locate/jpowsour

Short communication

Catalytic combustion of alcohols for microburner applications

Douglas A. Behrens, Ivan C. Lee*, C. Michael Waits

US Army Research Laboratory, Sensors and Electron Devices Directorate, 2800 Powder Mill Road, Adelphi, MD 20783, United States

ARTICLE INFO

Article history:
Received 7 August 2009
Received in revised form
30 September 2009
Accepted 1 October 2009
Available online 9 October 2009

Keywords:
Alcohols
Combustion
Microburner
Reforming
Electrospray
Bio-refinery

ABSTRACT

The combustion of energy dense liquid fuels in a catalytic micro-combustor, whose temperatures can be used in energy conversion devices, is an attractive alternative to cumbersome batteries. To miniaturize the reactor, an evaporation model was developed to calculate the minimum distance required for complete droplet vaporization. By increasing the ambient temperature from 298 to 350 K, the distance required for complete evaporation of a 6.5 μm droplet decreases from 3.5 to 0.15 cm. A platinum mesh acted as a preliminary measurement and demonstrated 75% conversion of ethanol. We then selected a more active rhodium-coated alumina foam with a larger surface area and attained 100% conversion of ethanol and 95% conversion of 1-butanol under fuel lean conditions. Effluent post-combustion gas analysis showed that varying the equivalence ratio results in three possible modes of operation. A regime of high carbon selectivity for CO_2 occurs at low equivalence ratios and corresponds to complete combustion with a typical temperature of 775 K that is ideal for PbTe thermoelectric energy conversion devices. Conversely for equivalence ratios greater than 1, carbon selectivity for CO_2 decreases as hydrogen, olefin and paraffin production increases. By tuning the equivalence ratio, we have shown that a single device can combust completely for thermoelectric applications, operate as a fuel reformer to produce hydrogen gas for fuel cells or perform as a bio-refinery for paraffin and olefin synthesis.

Published by Elsevier B.V.

1. Introduction

With the ever increasing technology a soldier is required to carry around on the battlefield comes an inevitable increase in the size and weight of the corresponding power source. Battery technology has made great strides in the past decades, resulting in new anodes, cathodes, and the ability to recharge them. However, batteries have an extremely small specific energy when compared to liquid fuels such as ethanol, butanol, and JP8. A typical lithium ion battery is roughly two orders of magnitude less dense than ethanol or butanol: 0.6 MJ kg^{-1} compared to 29.9 and 36.6 MJ kg^{-1}, respectively. If an efficient method for combusting these fuels at temperatures in the range of thermoelectric or other energy converting devices was developed, the power source could be drastically miniaturized which would significantly decrease the load a soldier must carry.

In this paper, we focus on two parameters critical to the process of miniaturizing a combustor: time/length scales for complete evaporation, and the effect of catalyst materials. The distance required for evaporation and the necessary path length over the catalyst for combustion, in addition to the distance needed for thorough vaporized fuel–air mixing, are three stages that dictate the overall length scale of a microburner. Decreasing any of those required lengths will allow for an overall decrease in microburner size. The time scale for evaporation was studied because complete evaporation is beneficial for the gas phase fuel and air to mix sufficiently for combustion on the catalyst. The catalyst material was investigated because different catalysts are more catalytically active (have shorter reaction time scales) than others and can produce higher conversions with lower surface areas. These smaller more effective catalysts require less space and can allow the microburner to decrease in size.

Alcohols such as ethanol and 1-butanol were chosen because they have several characteristics that are ideal for experimentation. They are easily renewable from biomass, and possess a simple chemical structure. The increase in energy density can only be capitalized on if the fuel is in the energy rich, liquid phase, at the conditions under which it is to be used. Ethanol and butanol are both liquids at room temperature and boil at 78.4 and 117.7 °C, respectively. The alcohols are single components, not a combination of components with different boiling points and viscosities. This enables simpler evaporation and diffusion models to predict their behavior. They burn clean: complete combustion results in the production of CO_2 and water. Neither of these combustion products poison the catalyst, so operation with the same catalyst can continue for longer periods of time. Also, they are electrically conductive enough that they can be injected using electrospray techniques [1], where a voltage difference applied between the

* Corresponding author. Tel.: +1 301 394 0292; fax: +1 301 394 1801.
E-mail address: ilee@arl.army.mil (I.C. Lee).

0378-7753/$ – see front matter. Published by Elsevier B.V.
doi:10.1016/j.jpowsour.2009.10.001

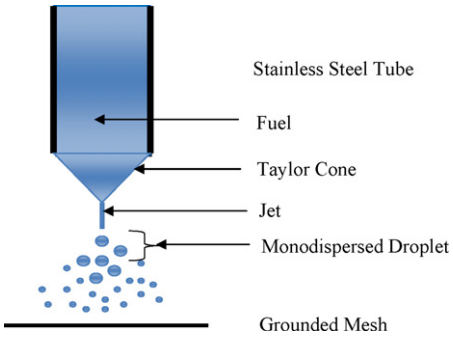

Fig. 1. Taylor cone depiction at steady state.

liquid fuel and a grounded mesh some distance away results in the formation of a Taylor Cone. When operated in cone-jet mode, charged liquid particles are emitted with a narrow droplet size distribution, which allows for a steady state evaporation rate to be established, and is shown in Fig. 1.

The combustion of ethanol and butanol occurs via Eqs. (1) and (2) shown below and are extremely exothermic.

$$C_2H_5OH + 3O_2 \rightarrow 2CO_2 + 3H_2O, \qquad \Delta H = -1407\,\mathrm{kJ\,mol^{-1}} \quad (1)$$

$$C_4H_9OH + 6O_2 \rightarrow 4CO_2 + 5H_2O, \qquad \Delta H = -2713\,\mathrm{kJ\,mol^{-1}} \quad (2)$$

The equivalence ratio (φ), the ratio of the actual fuel to air ratio divided by the stoichiometric fuel to air ratio, also plays an important role. A φ-value of unity signifies a stoichiometric feed of fuel and air, as shown in the above equations. The φ-value can be controlled by adjusting the amount of fuel and/or oxygen that are reacted. In the limit of high φ-values, the reaction is "fuel rich" and incomplete combustion occurs because not enough oxygen exists to combust the fuel. However, low φ-values indicate a "fuel lean" environment that has plenty of oxygen to oxidize the fuel into its combustion products: carbon dioxide and water.

The chemical kinetics of high temperature ethanol oxidation reactions has been exhaustively studied for temperatures ranging from 800 to 1600 K for equivalence ratios varying from 0.25 to 2 [1–4]. The experimental findings matched the predicted theory with remarkable agreement even over the extremely wide range of temperatures studied. Ethanol decomposition reaction pathways by pyrolysis, no oxygen present, have also been studied in depth for temperatures greater than 900 K [5,6]. Homogeneous gas phase flame-combustion reactions were carried out in the literature [7,8], but typical reactor wall temperatures for these types of reactions can exceed 1200 K; these temperatures are far too high for any economically viable energy conversion device. Catalytic combustion of a more complicated and energy dense hydrocarbon, JP8, achieved complete combustion for flowrates less than 5 mL h^{-1} at a maximum catalyst temperature of less than 900 K [9]. This indicated that the catalytic reactions not only initiate the reaction, but also play a large role in overall fuel conversion. Kyritsis et al. have also shown that miniaturizing the reactor requires use of a catalyst. This results from the larger surface effects that come with an increasing surface area/volume ratio as the overall size is decreased [10]. Without the catalyst to support the combustion at lower temperatures, the possibility exists that the larger convection forces would extinguish the reaction.

The optimization of catalysts for different fuels is also an active area of research. Experiments have been conducted with catalysts composed of thermally stabilized, ion-exchanged zeolite, palladium on stabilized alumina, and catalysts doped with Ce and Ni to better prevent sulfur poisoning when using JP8 [9,10]. In general, catalysts can lower the activation barrier of a reaction, thus allowing the reaction pathway to occur at lower temperatures. This is extremely advantageous because it allows for combustion temperatures between 650 and 850 K, which is ideal for PbTe–$Ge_{0.8}Si_{0.2}$ (5%) thermoelectric devices [12].

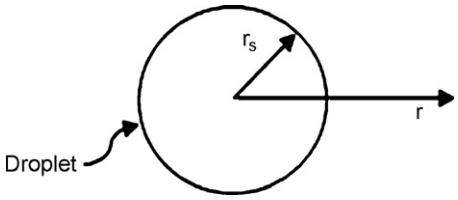

Fig. 2. Droplet with coordinate system.

Studies of catalytic reforming for C1–C3 alcohols have been done for C/O ratios greater than 1.0, and they report hydrogen gas selectivities of greater than 70% for ethanol [13,14]. The papers do not cover lower C/O ratios (corresponding to $\varphi < 3$) for any of the alcohols, but we studied a range of equivalence ratios from 0.19 up to 3.17 for both ethanol and butanol.

There are however, significant challenges that lie ahead before liquid fuels can be commercially viable. The lithium ion battery is widely used, not because of its size or weight, but because of its durability, ease of integration into many electronic technologies, and affordability. Liquid fuels need to become more reliably combustible, more rigid in structure, and have a consistent and efficient method to convert the reaction products into a usable form of energy before they can compete with batteries.

This paper begins by developing an evaporation model for ethanol and butanol. The model is then solved for experimental conditions to miniaturize the required time and distance for complete vaporization. The predictions of the model were then applied to the design of the reactor. Next, catalytic conversion data for ethanol and butanol are presented and catalyst efficiencies are discussed. Analyses of carbon and hydrogen selectivities for ethanol and butanol, respectively follow, and comparisons of the fuels as candidates for hydrogen gas production were considered.

2. Approach

2.1. Evaporation model of a liquid droplet

In order to predict the evolution of the droplet size with time, the Stefan Problem's differential mass balance was solved for a binary species in a spherically symmetric coordinate system with the radius being the only coordinate variable as shown in Fig. 2 [15].

Using the droplet mass conservation, the change in droplet mass, m_d, with time is equal to the rate at which the liquid is vaporized:

$$\frac{dm_d}{dt} = -\dot{m} \quad (3)$$

Here, $\dot{m}$ represents the evaporation rate and is attained, in part, by assuming that at the droplet surface, the vapor mass fraction is $Y_{A,s}$. This is shown here:

$$\dot{m} = 4\pi r_s \rho D_{AB} \ln\left(\frac{1 - Y_{A,\infty}}{1 - Y_{A,s}}\right) \quad (4)$$

where r_s represents the droplet radius at the surface, ρ represents the gas density, D_{AB} represents the binary diffusion coefficient, and the vapor fraction at the droplet surface and an infinite distance away are $Y_{A,s}$ and $Y_{A,\infty}$, respectively. The mass of the droplet is simply the volume multiplied by the density. Plugging both this relationship, as well as Eq. (4), into Eq. (3) and rearranging yields

the following differential equation:

$$\frac{dD^2}{dt} = -\frac{8\rho D_{AB}}{\rho_l}\ln(1+B_y) \quad (5)$$

Here the natural log term $(1+B_y)$ was rewritten from the natural log term $(1-Y_{A,\infty})/(1-Y_{A,s})$ seen in Eq. (4). The dimensionless transfer number, B_y, can be interpreted as a "driving potential" for mass transfer [15]. Then, by defining the right hand side of Eq. (5) as a constant K, the equation can be integrated with the appropriate boundary conditions and has the following solution:

$$D^2(t) = D_o^2 - Kt \quad (6)$$

Eq. (6), also known as the d^2-law, shows that setting a D value of zero, and solving for t would represent the time it takes for the droplet to completely evaporate. The main assumption is that droplet temperature is uniform and does not exceed the boiling point of the liquid. This assumption eliminated the need to apply an energy balance to the liquid droplet or the gas envelope surrounding the droplet, greatly simplifying the number of equations and unknowns in the process.

2.2. Experimental approach of fuel combustion

A grounded mesh was placed a distance of 1 cm below the droplet source (a stainless steel tube) in a cylindrical quartz reactor, and the catalyst was located 12.5 cm below the bottom of the grounded mesh. The inner diameter of the quartz tube reactor was 2 cm. Nitrogen and oxygen gases were introduced near the top of the reactor and the effluent gas was sent to the GC through the bottom of the reactor. An inert foam mixer was placed below the grounded mesh to aid in providing nitrogen and oxygen flow uniformity. This foam also aided in mixing the fuel vapor and incoming nitrogen and oxygen gases. Liquid fuel entered the reactor via the stainless steel tube (outer diameter of 1.70 mm and inner diameter of 1.20 mm) and was electrosprayed in cone-jet mode by creating a voltage difference between the droplet source and a neutral grounded mesh (~3300 V). Care was taken to make certain that the grounded mesh was perpendicular to the direction of the droplet trajectory so as to create a uniform electric field. Sufficient heat was supplied via heating tape to the grounded mesh (generally a couple degrees above the boiling point of the fuel) to ensure complete evaporation in accordance with the predictive model.

The catalyst material was placed between two inert, porous alumina supports that acted as heat shields and also served as another mixing layer to ensure uniform fuel vapor concentration over the entire catalyst surface. Details of the reactor setup are depicted in Fig. 3. A platinum metal mesh or a Rh/Al_2O_3 foam was used as the catalyst. The platinum metal mesh weighed about 0.50 g and was roughly 0.5 mm thick. The Rh/Al_2O_3 foam (5 mm thick) contained 0.061 g of Rh and was prepared in the manner detailed in the literature [11]. The alumina monolith foam (Vesuvius, 80 ppi, 17 mm diameter, 5 mm thick) was coated with γ-alumina to roughen the foam surface and to increase the surface area. Then the foam was calcined in a box furnace at 700 °C for 15 h. An aqueous $Rh(NO_3)_3$ solution was added to the foam, and the resultant foam was calcined in the box furnace at 700 °C for another 15 h.

Since analysis of the combustion products is crucial to understanding the results of the operating conditions, an air tight seal was needed around the combustor and gas chromatograph (GC). The amounts of hydrogen, oxygen, nitrogen, carbon monoxide, carbon dioxide, methane, acetylene, ethane, ethylene, propane, propylene, butane, 1-butene, cis-2-butene, and trans-2-butene were monitored by an Agilent 4-channel micro-GC. Before each experiment, nitrogen gas was passed through the reactor in order to clear out any lingering gases, check to make sure there was no leak, and

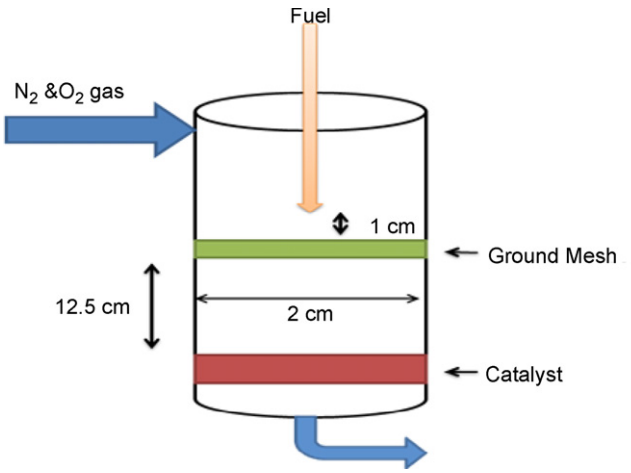

Fig. 3. Schematic diagram of the reactor set up for the alcohol combustion.

to ensure that no oxygen was present. Heating tape was activated to provide heat to the catalyst and the region between the fuel atomizer and the grounded mesh. Then the appropriate nitrogen and oxygen flowrates were introduced, and the ground and catalyst temperatures were allowed to equilibrate. Next, the voltage differential between the ground and the stainless steel tube was established for electrospray, and the fuel flow was initiated. Voltages were then adjusted to maintain electrospray stability in cone-jet mode as needed. The ground and catalyst temperatures were again allowed to reach a steady state operating temperature and the GC recorded the gas composition during this time.

When comparing ethanol and butanol, the experiments were run at the same equivalence ratios. This set the total oxygen flowrate, and then the nitrogen flowrate was adjusted so that the total volumetric flowrate of gas remained the same. This guaranteed that the residence time inside the reactor was the same for both fuels. An alternative approach would be adjusting the fuel feed rate between ethanol and butanol to produce the same power load (heat release, hence adiabatic and catalyst temperature) for the equivalent flow of N_2/O_2 mixture for both fuels. This approach will give different residence times but the same catalyst temperatures for ethanol and butanol oxidation at each equivalence ratio. The authors recognized the significance of this alternative approach, and reaction kinetics of alcohol oxidation will be further studied in another study with this approach.

Fuel flowrates of 1 mL h^{-1} were used. Using the equation developed in Ganan-Calvo et al. [16], the mean droplet diameter for ethanol at this flowrate was estimated to be 6.5 μm and was verified experimentally using Phase Doppler Particle Analysis (PDPA) measurements. The model predicted a butanol droplet diameter within 0.5 μm of the ethanol droplet diameter, but PDPA analysis was not performed.

For this paper, conversion was defined based on a carbon balance. The carbon atoms in all of the products were summed, and were then divided by the total amount of carbons in the fuel (ethanol or butanol) fed into the reactor. This represents the percentage of carbon atoms that were converted into some compound other than the fuel.

Carbon selectivity was defined as the number of carbon atoms in a particular species, divided by the total number of carbon atoms in the product gas as shown:

$$\text{C atom selectivity} = \frac{\#\ \text{C in species } X}{\sum \text{C in product}} \quad (7)$$

Similarly, hydrogen selectivity was defined as the number of hydrogen atoms in a particular species divided by the total number

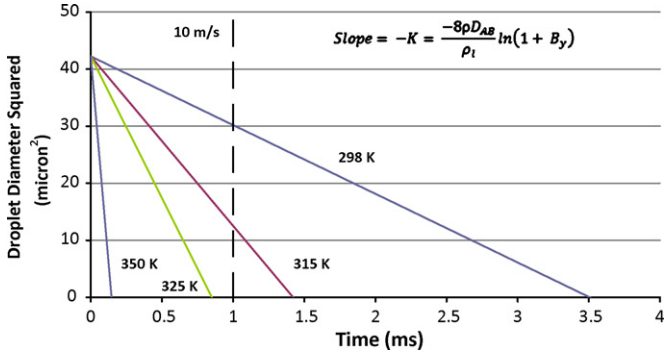

Fig. 4. The d^2-law model for ethanol droplet.

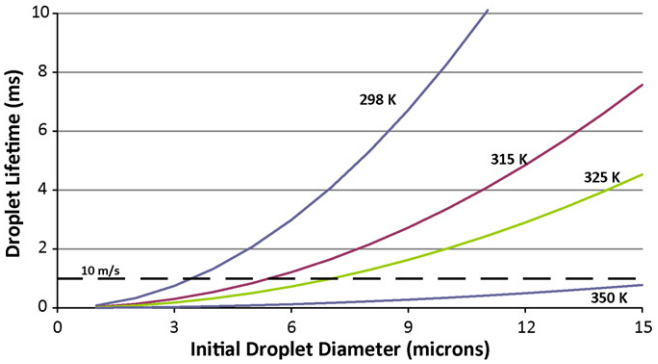

Fig. 5. Droplet lifetime as a function of initial droplet diameter for ethanol.

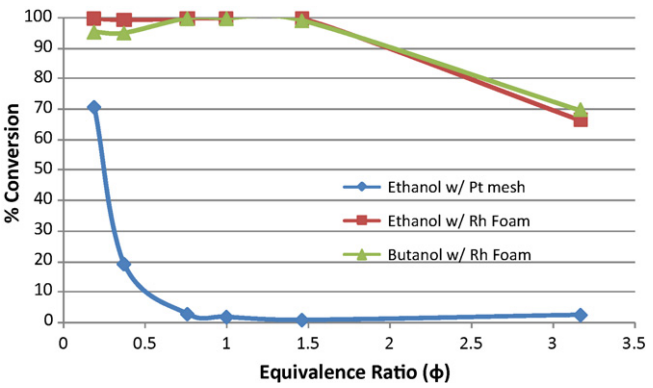

Fig. 6. Ethanol and butanol conversion with Pt mesh and Rh/Al_2O_3 foam catalysts.

of hydrogen atoms in the product gas. This represents the percentage of converted hydrogen atoms in each of the species studied and is analogous to Eq. (7) if hydrogen is substituted for carbon.

3. Results and discussions

3.1. Evaporation of an ethanol droplet

Complete evaporation of ethanol droplets before hitting the grounded mesh would provide good fuel–air mixing prior to combustion. PDPA measurements showed that the initial mean droplet size coming out of the stainless steel tube used for the experiment were roughly 6.5 μm in diameter and had an average velocity of approximately 10 m s^{-1}. Accordingly, Eq. (6) was solved for a 6.5 μm ethanol droplet at various temperatures and was plotted in Fig. 4.

Fig. 4 shows the droplet evolution as a function of time for an ethanol droplet with an initial diameter of 6.5 μm (42.25 μm^2) for temperatures ranging from room temperature up to the boiling point of ethanol. Each line follows a single droplet from its initial release until complete evaporation (intersection with the x-axis). The black dash indicates the time it would take for a droplet traveling at 10 m s^{-1} (anticipated velocity) to cover the 1 cm gap and reach the grounded mesh. The graph shows that at room temperature the droplet requires 3.5 ms, corresponding to 3.5 cm, to fully vaporize before hitting the grounded screen, whereas a temperature of 350 K achieves complete evaporation in 0.1 ms, or 0.1 cm. Since the operating temperature for the reactor is right around the boiling point of ethanol, about 350 K, the model ensures that the droplet will be completely vaporized. This slight increase in temperature results in a reduction of required evaporation distance by more than a factor of 10.

3.2. Effects of initial droplet size

The evaporation model can also predict the droplet lifetime as a function of initial droplet diameter, as shown in Fig. 5. Each point displayed on the graph represents the extinction of a droplet for a given droplet diameter at the particular temperature. This allowed the design of the reactor to be optimized for a given initial droplet diameter and droplet velocity. The dashed line again represents how long it would take for a droplet moving at 10 m s^{-1} to reach the grounded mesh positioned 1 cm away. The model predicts that for a droplet diameter of less than 3.5 μm, achievable using multiplexing as in Deng et al. [17], the droplet would be evaporated over the entire range of temperatures shown. Conversely, for an initial droplet size of 12 μm, only a temperature of 350 K would result in complete evaporation before the grounded screen. This was used to determine what temperature was needed in order to ensure complete evaporation for the given initial droplet diameter and 1 cm spacing. Together these graphs obtained from the model drove the design considerations by limiting how small the microreactor could be based on droplet diameters and operation temperatures, as well as how much heat circulation was required.

Using a heat of vaporization of 51 kJ kg^{-1}, and assuming that the binary diffusivity constant of butanol in air is similar to that for ethanol, the model predicts that butanol will fully evaporate in 0.1 cm at a temperature of 391 K (the boiling point of butanol). Thus butanol will vaporize fully before it hits the grounded mesh, and the lack of condensation on the mesh verifies that the model prediction holds for both ethanol and butanol.

3.3. Conversion of ethanol and butanol combustion

Ethanol combustion data were obtained for both the platinum metal mesh and Rh/Al_2O_3 foam catalysts whereas the Rh/Al_2O_3 foam was the only catalyst used for butanol combustion. Platinum mesh was selected because of its use as a generic catalyst for many applications, whereas the rhodium foam was chosen because of its high catalytic activity for alcohol oxidation [12,14]. Fig. 6 shows that the Rh/Al_2O_3 foam catalyst is superior to the Pt mesh for combusting ethanol. This result was expected, and the platinum mesh was not used after the initial comparison to the rhodium foam using the same fuel. The foam was able to achieve almost 100% conversion for low equivalence ratios while maintaining greater than 60% conversion at high equivalence ratios (excess fuel). The back-face catalyst temperature was between 703 and 853 K. On the other hand, the platinum mesh was only able to achieve 70% conversion at very low equivalence ratios, but the conversion quickly decreased to less than 5% as the fuel to air ratio was increased. This trend is likely due to the higher catalytic activity of the Rh/Al_2O_3 foam, as well as the fact that the Rh particles were well-dispersed on the alumina foam to give a larger surface area for reactions to take place. Since two

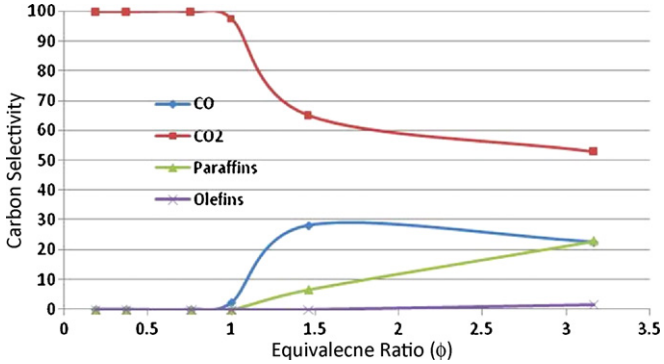

Fig. 7. Carbon selectivity for ethanol with a Rh/Al_2O_3 foam catalyst as a function of equivalence ratio.

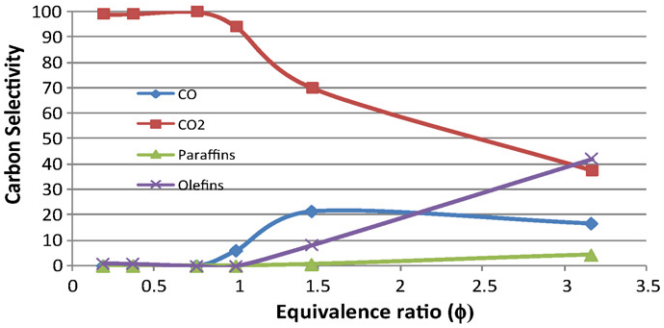

Fig. 8. Carbon selectivity for butanol with a Rh/Al_2O_3 foam catalyst as a function of equivalence ratio.

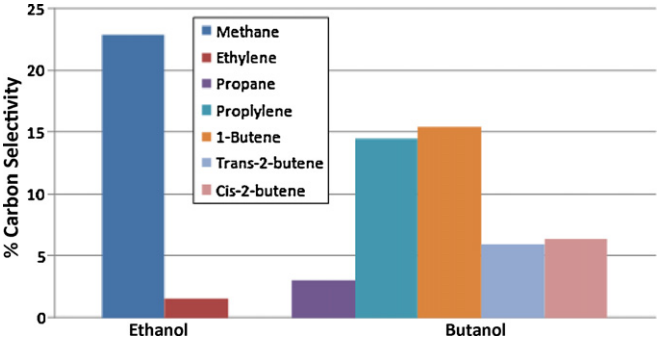

Fig. 9. Comparison of carbon selectivities for ethanol and butanol conversions at an equivalence ratio of 3.17.

variables were changed when the catalysts were switched, it cannot be determined whether the increased conversion was due to the larger surface area, higher activity, or a combination of the two.

3.4. Carbon selectivity of ethanol and butanol combustion products

Fig. 7 displays the carbon selectivities of ethanol combustion for carbon monoxide, carbon dioxide, paraffins, and olefins with increasing equivalence ratios. This shows that two distinct regimes exist for carbon selectivity. At low equivalence ratios ($\phi < 1$), where excess oxygen is present, the selectivity of carbon to CO_2 is 100%. This is partly due to the fact that any CO produced will be immediately oxidized by the excess oxygen into CO_2. If CO_2 is produced, that means that combustion is occurring and that water is the other product. Since those are the only products produced at low equivalence ratios, this is the regime of complete combustion. As the equivalence ratio approaches unity, that is there are 3 moles of oxygen for every mole of ethanol (Eq. (1)), the selectivity of carbon for CO_2 starts to decrease. As the ratio of ethanol to oxygen is increased further, more carbon monoxide, methane, and even ethylene are produced as the carbon selectivity of carbon dioxide decreases. The appearance of significant amounts of CO indicates that the fuel is now being reformed into CO and H_2 (syngas). This has strong possibilities for applications in fuel cells. A solid oxide fuel cell has a higher operating temperature and is more CO tolerant than a proton exchange membrane fuel cell. The poisonous CO can be easily converted to CO_2 and more H_2 with a water gas-shift catalyst, or can be directly used in a solid oxide fuel cell.

The chemistry behind the catalyst surface reactions that result in production of the gases mentioned above has been studied extensively in the literature, but in particular ethanol adsorption and subsequent decomposition on a rhodium surface was investigated [18]. Houtman and Barteau found that ethanol initially forms an ethoxy species on the surface of the catalyst before creating a bridged oxametallacycle. This then undergoes C–C bond scission, and is broken down into H, C, and O atoms that then recombine to produce syngas. Information about similar pathways for butanol was sparse in the literature, and experiments with other four carbon alcohols will shed light on a possibly analogous mechanism to the one for ethanol.

The carbon selectivity data for butanol combustion is depicted in Fig. 8 in an analogous manner to Fig. 7. Fig. 8 shows the carbon selectivity for butanol combustion, and the trend is very similar to that of ethanol shown in Fig. 7. CO_2 has a nearly 100% carbon selectivity until the stoichiometric fuel to air ratio is approached. After that, the CO_2 selectivity rapidly decreases to a final value of less than 40%. Comparison of Figs. 7 and 8 shows that the carbon selectivity for CO_2 decreases much further for butanol than for ethanol combustion, and this corresponds to larger amounts of other products being formed.

About 60% of the carbons for butanol combustion compared to only about 45% of the carbons in ethanol combustion are found in a compound other than CO_2 at an equivalence ratio of 3.17. At this equivalence ratio the catalyst temperatures were 654 and 700 K for ethanol and butanol reactions, respectively. Approximately 25% and 45% of the carbons for ethanol and butanol combustion, respectively are in the form of paraffins and olefins as shown in Fig. 9. The comparison also indicates that olefins (14.5% propylene, 15.5% 1-butene, 6.0% trans-2-butene and 6.5% cis-2-butene) are produced for butanol combustion in significant amounts, whereas only trace amounts of olefins (0.57% ethylene) were produced for ethanol combustion. The converse is true of paraffins; more paraffins are found for ethanol than are found for butanol combustion. The carbon selectivities are 22.9% methane in ethanol combustion and only 3.1% propane in butanol combustion. This conversion of fuel into paraffins and olefins has promise for use in bio-refinery technologies also, however further research needs to be conducted in order to fully understand the mechanism that would allow for optimization of the operating conditions.

3.5. Hydrogen selectivity of ethanol and butanol combustion products

Fig. 10 depicts the hydrogen selectivity for ethanol combustion, and shows that nearly all of the hydrogen atoms are present as water vapor at low equivalence ratios ($\phi < 1$). Then, as the stoichiometric ratio is approached and the equivalence ratio increases further, more hydrogen gas and paraffins were produced as less and less water vapor is formed. However, even at equivalence ratios greater than 3, the hydrogen selectivity for water vapor is still around 70%. Hydrogen selectivity for H_2 peaked at 18% and occurred for an equivalence ratio of roughly 1.5. Hydrogen selectivity for paraffins was the highest at the largest equiv-

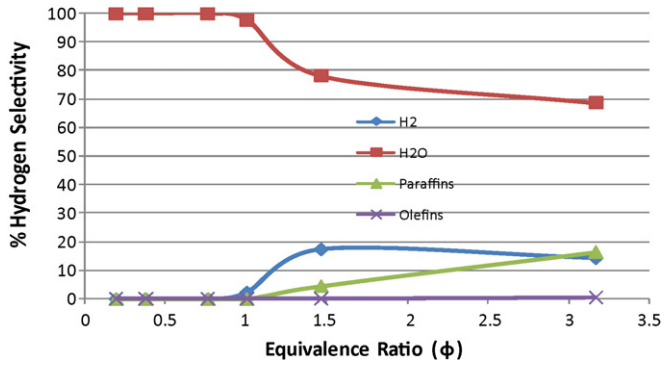

Fig. 10. Hydrogen selectivity for ethanol with a Rh/Al_2O_3 foam catalyst as a function of equivalence ratio.

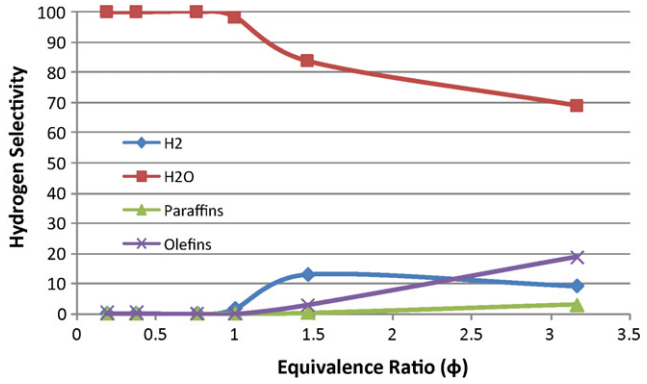

Fig. 11. Hydrogen selectivity for butanol with a Rh/Al_2O_3 foam catalyst as a function of equivalence ratio.

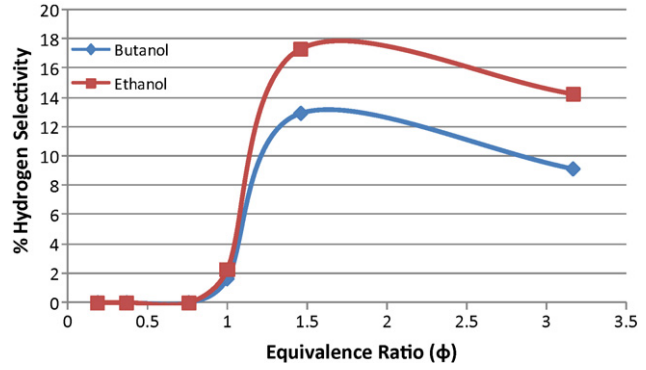

Fig. 12. Hydrogen selectivity for ethanol and butanol with a Rh/Al_2O_3 foam catalyst as a function of equivalence ratio.

alence ratio studied, and only trace amounts of olefins were detected.

The hydrogen selectivity for butanol combustion is shown in Fig. 11. The results look strikingly similar to the hydrogen selectivity for ethanol combustion. The hydrogen selectivity for water vapor begins to decrease around the stoichiometric ratio, and again decreases to a final value of around 70%. Hydrogen gas selectivity increased for ϕ-values greater than one, and then decreased slightly to a final value of between 15% and 10%, respectively for ethanol and butanol combustion. The main difference is the amount of olefins and paraffins produced as discussed in the previous section. Ethanol combustion produced a hydrogen selectivity of nearly 20% paraffins and no olefins at a φ-value of 3.17, whereas butanol combustion produced a hydrogen selectivity of slightly less than 20% olefins and about 3% paraffins.

Fig. 12 compares the hydrogen selectivity for ethanol and butanol as a function of equivalence ratio for the Rh/Al_2O_3 foam catalyst. This graph indicates that ethanol combustion produces a higher hydrogen selectivity for H_2 gas at all equivalence ratios. Thus ethanol is better suited for fuel reformation than butanol over the range of equivalence ratios studied. More importantly, an optimum equivalence ratio of approximately 1.5 produces the highest hydrogen selectivity for both ethanol and butanol. At this equivalence ratio the catalyst temperatures were 706 and 779 K for ethanol and butanol reactions, respectively. This would be an ideal equivalence ratio at which to operate if H_2 production for fuel cells was required.

4. Conclusions

An evaporation model was used to predict the behavior of ethanol droplets at varying temperatures. This model limited how small the reactor could be made based on the velocity of the fuel droplets and the temperature of operation. From this, the temperature required to evaporate a droplet of a given initial diameter was calculated to make sure that it fully vaporized before reaching the grounded mesh so that proper fuel/air mixing could occur. The micro-combustor was then shown to be able to produce complete combustion products and the associated high temperatures for pairing with thermoelectric devices at low equivalence ratios. The same device can also be used to achieve fuel reformation for fuel cells at higher equivalence ratios by changing only the fuel to air ratio. At even higher equivalence ratios, paraffin and olefin production becomes significant and could be used as part of a bio-refinery process.

Acknowledgement

The authors thank Dr. Brian Morgan at US Army Research Laboratory for his helpful input during the preparation of this manuscript.

References

[1] K. Tang, A. Gomez, J. Colloid Interface Sci. 184 (1996) 500–511.
[2] M.P. Dunphy, P.M. Patterson, J.M. Simmie, J. Chem. Soc. 87 (1991) 2549–4559.
[3] J. Li, A. Kazakov, M. Chaos, F.L. Dryer, Chemical kinetics of ethanol oxidation, in: 5th US Combustion Meeting, San Diego, 2007, p. C26.
[4] T.S. Norton, F.L. Dryer, Int. J. Chem. Kinet. 24 (1992) 319–344.
[5] J. Li, A. Kazakov, F.L. Dryer, J. Phys. Chem. 108 (2004) 7671–7680.
[6] A.A. Borisov, V.M. Zamanskii, A.A. Konnov, V.V. Lisyanskii, S.A. Rusakov, G.I. Skachkov, Sov. J. Chem. Phys. 9 (1992) 2527–2537.
[7] E.K. Anderson, J.A. Koch, D.C. Kyritsis, Combust. Flame 154 (2008) 624–629.
[8] S. Parag, V. Raghavan, Combust. Flame 156 (2008) 997–1005.
[9] D.C. Kyritsis, B. Coriton, F. Faure, S. Roychoudhury, A. Gomez, Combust. Flame 139 (2004) 77–89.
[10] A. Gomez, J.J. Berry, S. Roychoudhury, B. Coriton, J. Huth, Proc. Combust. Inst. 31 (2007) 3251–3259.
[11] I.C. Lee, Catal. Today 136 (2008) 258–265.
[12] J.R. Sootsman, J. He, V.P. Dravid, C. Li, C. Uher, M.G. Kanatzidis, J. Appl. Phys. 105 (2009) 083718.
[13] E.C. Wanat, B. Suman, L.D. Schmidt, J. Catal. 235 (2005) 18–27.
[14] J.R. Salge, G.A. Deluga, L.D. Schmidt, J. Catal. 235 (2005) 69–78.
[15] S.R. Turns, An Introduction for Combustion, 2nd ed., McGraw-Hill, Boston, 2006.
[16] A.M. Ganan-Calvo, J. Davila, A. Barrero, J. Aerosol Sci. 28 (1997) 249–275.
[17] W. Deng, J.F. Klemic, X. Li, M.A. Reed, A. Gomez, Proc. Combust. Inst. 31 (2007) 2239–2246.
[18] C.J. Houtman, M.A. Barteau, J. Catal. 130 (1991) 528–546.